Journal of Engineering and Sustainable Development
Vol. 29, No. 04, July 2025
https://jeasd.uomustansiriyah.edu.iq/index.php/jeasd
ISSN 2520-0917
Research Article
https://doi.org/10.31272/jeasd.2818

Scanning Technologies Adoption for Transtibial Residual Limb Shape Characterization

Sarah Duraid AlQaissi[1*], Ahmed A.A. AlDuroobi[1], Abdulkader Ali. A. Kadaw[2]

[1]Department of Prosthetics and Orthotics, College of Engineering, Al-Nahrain University, Baghdad, 10070, Iraq
[2]TU Bergakademie Freiberg, Institute for Machine Elements, Engineering Design and Manufacturing, 09599, Freiberg, Germany

[*]Email: st.sara.d.dawood.msc@ced.nahrainuniv.edu.iq

Article Info

Received	**30/06/2024**
Revised	**27/03/2025**
Accepted	**18/05/2025**

Abstract

In prosthetics, 3D scanning technology plays a crucial role in gathering data for designing prosthetic devices. New tools for capturing the external shape of human body parts are rapidly emerging. This study conducted a comparative analysis to assess the accuracy and precision of two handheld 3D scanners, including the Peel 3 3D scanner and a smartphone application, in scanning the residual limb of a transtibial participant. The residual limb was manually measured, and six scans were taken with each scanning system, compared to the reference computed tomography (CT) model. A repetition test was performed to determine the mean value and standard deviation of the scanned models in VXelements software for comparison purposes. The results showed a standard deviation difference between the Peel 3 and CT scans ranging from ± 0.828 to 0.907mm, and from ± 0.823 to ± 0.877mm for the smartphone scans. The repetition test indicated standard deviations ranging from ± 0.531 to 0.599 mm for the Peel 3 and ± 0.458 to 0.690 mm for the smartphone. This analysis evaluated the accuracy of the 3D scanners and identified the essential specifications for their effective use in prosthetics.

Keywords: Accuracy; Peel 3 Scanner; Precision; Smartphone 3D Scanning; Transtibial Amputation

1. Introduction

In prosthetics, the integration of cutting-edge technologies has revolutionized the way prosthetic devices are designed and customized to meet the unique needs of individuals with limb differences. One such technology that has garnered significant attention and acclaim is 3D scanning. This advanced method of capturing precise measurements and creating detailed models is pivotal in enhancing the overall prosthetic fitting process and improving patient outcomes [1]-[3].

One of the primary advantages of (3D) scanning in prosthetics is its ability to offer a contactless approach to data collection. Unlike traditional methods, 3D scanning provides a non-invasive, faster, and more detailed method of capturing the exact contours of a residual limb. This contactless nature not only enhances patient comfort during the scanning process but also ensures greater accuracy in capturing critical data points essential for designing prosthetic devices [4],[5], where the marriage of 3D scanning technology with advanced computer processing capabilities has ushered in a new era of innovation in prosthetics. By transforming scanned data into intricate 3D models, 3D scanning eliminates the need for labour-intensive gypsum positives traditionally used in prosthetic design [3],[6],[7]. Recent research has unequivocally demonstrated the reliability and efficacy of 3D scanning for obtaining crucial data in prosthetics. 3D scanning technology's precision and reliability have established it as a reliable tool within the prosthetic field, utilised for various purposes ranging from initial evaluations to complete fittings. Prosthetists and researchers rely on the precision of 3D scanning to ensure optimal patient outcomes, underscoring its importance in modern prosthetic practices [8]-[11].

Comparative studies have shed light on the versatility and cost-effectiveness of different 3D scanning solutions by comparing high-end and low-cost 3D scanners [12]-[14]. Farhan et al. identify the potential for utilizing affordable scanning technologies for specific applications and highlight the accessibility of 3D scanning [15]. A new development in prosthetics and orthotics practice is the integration of smartphones and specific 3D scanning applications into the field of 3D scanning [16]. Leveraging the sophisticated True Depth cameras in modern smartphones [17]-[19], these applications offer a portable and user-friendly solution for capturing detailed limb measurements. The convenience and accessibility of smartphone-based 3D scanning have opened up new avenues for enhancing prosthetic design processes and improving patient care. Research has underscored the remarkable precision and accuracy smartphone apps equipped with 3D scanning capabilities can use to capture body measurements. Therefore, it became necessary to prove the ability of these techniques and applications to provide detailed and reliable data points showcasing their potential in the prosthetics field, particularly for transtibial amputees, thus proving their usefulness in producing comfortable sockets. The primary objectives of this research are to assess the accuracy and precision of Peel 3 and smartphone-based 3D scanners, compare these technologies to traditional CT scanning as a reference model, and identify each technique's potential advantages and limitations.

2. Methods and Materials

This study compares the surface precision of 3D models obtained through 3D scanning, specifically, a residual limb model of a 23-year-old male patient with transtibial amputation in the left leg with 62 kg in weight, 168 cm height, and K4 activity level. The K4 activity level refers to an individual capable of high-impact activities, such as sports or manual labor, making it critical to ensure accurate and durable prosthetic fittings. The cause of amputation is trauma, and the amputation level is medium. Also, the stump was free from wounds, and there was no painful area. Through the study, the patient received a fully assembled prosthetic limb at no cost, in addition to a silicone liner system (ALPS, Cushion Liner, Grip Gel) with a 6 mm thickness (SPFR26-6), in place of the previous one.

In this research, the accuracy of the scanners was evaluated using a model obtained from a Computed Tomography (CT) scan, which serves as the reference model. Magnetic Resonance Imaging (MRI) was also conducted. The practical models were created using affordable 3D scanning systems, such, as the Creaform Peel 3 3D scanner from (Creaform Inc., Lévis, Quebec, Canada), and smartphones like iPhone X, Xs, Xs Max, Xr 11 11 Pro and 11 Pro Max from (Apple Inc., Cupertino, CA, USA). These devices were equipped with a TrueDepth camera for scanning. The scanning process involved an app called Comb that is recommended for Prosthetics and Orthotics (P&O) applications. Fig. 1 outlines the research steps starting with reconstructing the model of the stump obtained from CT/MRI imaging, including (the internal bones, flesh, and external residual limb structure), in addition to the usage of the Peel 3 scanner and Comb scan to capture the limb's external surface.

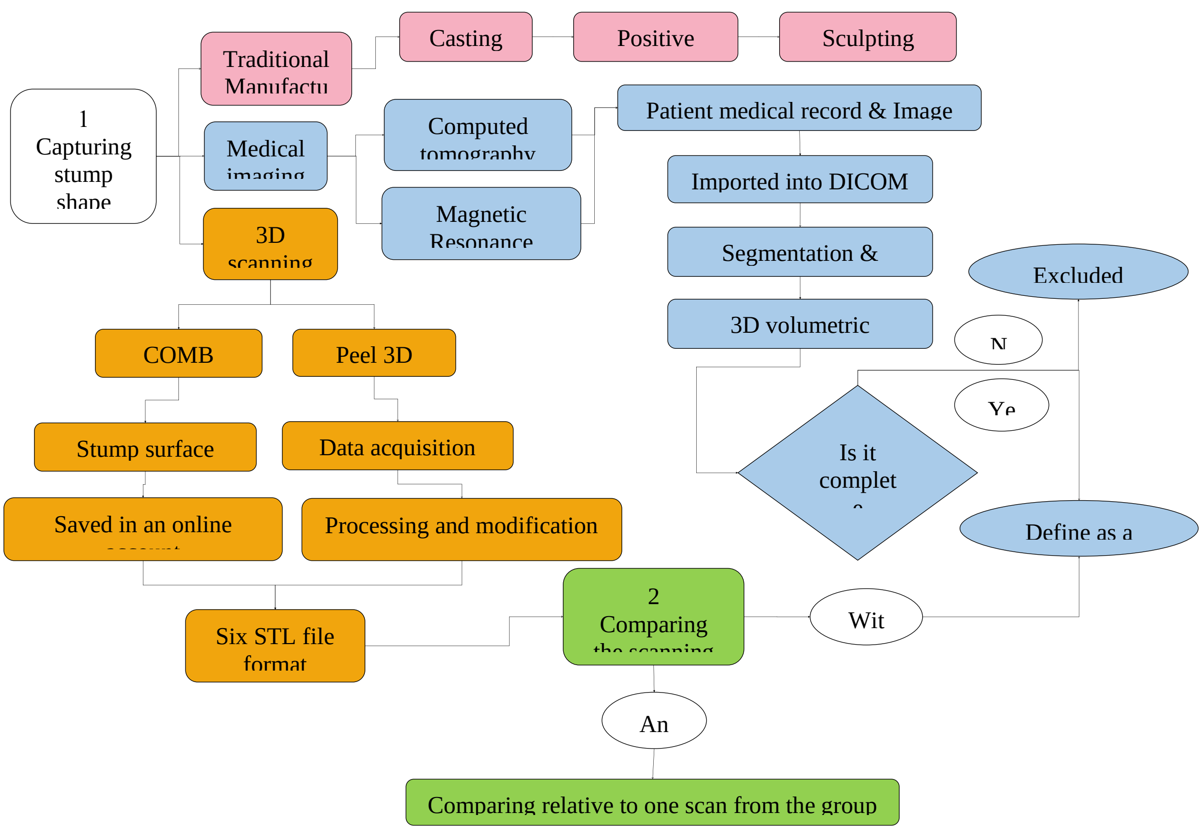

Figure 1. The fundamental steps of the research methodology.

Throughout the process of capturing the limb, challenges regarding the 3D geometric reconstruction were encountered involved ensuring the positioning of the patient and stump during acquisitions, the definition of the marker's points on the stump for reference and devising the alignment strategies for various digital models to establish a protocol with the necessary precision for socket production. Attention was paid to biomechanical factors that significantly influence the accuracy of the virtual model. The next step involves comparing models generated by each scanning system. These systems are divided into two groups, each consisting of six scans that were consistently compared based on a scan from their group. Subsequently, a comparison between models from both groups was done against a reference CT scan.

2.1. Capturing Stump Shape

2.1.1. Traditional method

Traditional methods used in creating sockets often require a hands-on and detailed approach. In these methods, prosthetic experts must understand the shape of the amputee's residual limb and make educated assumptions that impact how well the socket fits. The process involves steps, including comparing measurements of the sound limb with the measurements on the residual limb. Additionally, a qualitative assessment is conducted on factors like muscle strength, joint function, skin condition, scarring, pain location in the stump, and overall limb condition. Accurate measurements are taken around the patellar level and at one-inch intervals towards the end of the stump to determine stump size. Similarly, measuring from the patella point to the end of the stump to determine the residual limb length. Callipers are used to measure anterior-posterior (AP) and medial-lateral (ML) diameters in the directions of the condylar level and the patellar tendon level. After taking these measurements, casting or moulding procedures are typically carried out as shown in (Fig. 2C), which start by wrapping the patient's residual limb via cellophane to isolate the liner from the rest of the materials that will be added. Then, the process of creating a mould begins by wrapping plaster of Paris (Pop) bandages around the patient's stump, and the mould is made by wetting the (Pop) in water. This step captures the shape of the stump and forms a mould that replicates the topographic shape of the stump. The prosthetist applies pressure to areas of the stump that can handle it well to ensure weight distribution across those regions. The socket model is adjusted manually as depicted in (Fig. 2H) to improve the weight transfer from the bones to the prosthetic socket.

After that, in the sculpting process, the prosthetic professional adjusts how materials are distributed to improve pressure distribution and reduce pressure on spots like the tibial apex and other prominent bony areas marked before in the casting process. These spots are kept uncompressed to avoid pressure on the limb inside the socket, emphasizing how crucial it is to achieve a comfortable and stable fit of the prosthetic device. The traditional modification methods of the plaster rely heavily on expertise, skill, and artistic judgment. As a result, current socket design and fitting procedures are mostly subjective, leading to wide variations. After tuning the mould, the production of the prosthetic socket begins.

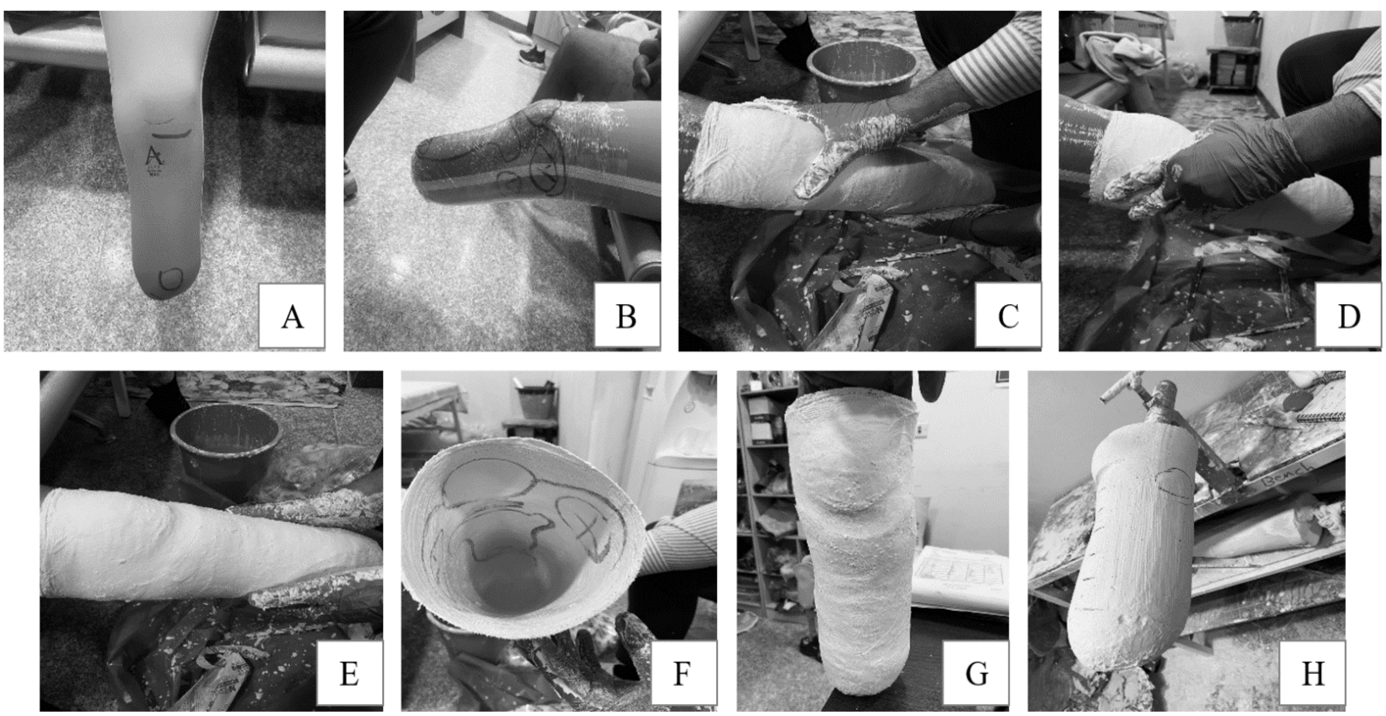

Figure 2. (A and B) The individual was seated during the casting process, with cellophane covering the residual limb with liner. (C) Plaster of Paris (POP)was then put on. (D) Indentations were identified by pressing both sides of the kneecap tendon and above the knee joint. (E and F) After removal. (G) The harmful mould was used to form the positive mould once it dried. (H) The positive mould was generated and shaped.

2.1.2. Medical imaging

CT acquisition has been performed using high-end professional SOMATOM Sensation 16 (Siemens AG, Medical Solutions, Forchheim, Germany) T1 0.5 at Baghdad Scan Medical Centre, by Dr. A.G. in Baghdad. The CT procedure specifications to produce a 2D DICOM (Digital Imaging and Communications in Medicine) file format with the following values: slice thickness 0.75 mm, Kernel B20f smooth, scan time 23.29s, and delay 4s. After processing the DICOM data, it was converted to a bitmap (BMP) format using RadiAnt DICOM Viewer 2023.1, Poznan, Poland, developed by the Medixant company.

For stabilizing the residual limb in a specific position of knee flexion at 5 degrees during CT acquisitions, supports were incorporated into the CT acquisition apparatus and placed under the thigh of the patient to increase control. Additionally, given the widespread availability of CT technology and the preference of orthopaedic surgeons for CT scans over MRI scans in characterizing the bone structure, the outer surface representing the skin boundary can be segmented from the CT image by fine-tuning the grey levels to delineate an area lower than the skin but higher than the background. This means the grey level setting should be minimized to differentiate the skin from the dark background, which provides ease in isolating anatomical components for analytical purposes.

Afterwards, the DICOM file is 3D reconstructed using a medical imaging program (InVesalius 3.1.1, Centre for Information Technology Renato Archer—CTI, Brazil). The following 3D volume reconstruction resulted in a highly accurate model of the 3D bone reconstruction and the external surface. Then, the model is exported in a file format (stereolithography STL).

For MRI scanning, a 1,5 Tesla Signa Excite GE Medical Systems was used in Baghdad Scan Medical Centre by Dr. A.G. in Baghdad. The test parameters were settled with the following values: FOV 23x23 cm, bitmap dimension 256x256 pixel obtained using a sequence with Repetition Time (RT) = 5.052 (ms), Echo Time (ET) =2.42 (ms), scan time 4 (min), slice thickness 3.0 (mm), the distance between images = 0.6 (mm), and the series description was T1 3D Axial. Images were captured using a phased array surface coil wrapped around the limb. When focusing on a particular body part during scanning, the MRI device produces images sliced according to its settings and the desired level of intricacy. Every single slice of data is stored in the DICOM format.

All DICOM data were exported to the application for processing and displaying medical images (RadiAnt DICOM Viewer 2023.1, Poznan, Poland), developed by the Medixant company. MRI slices were affected by noise due to the artifact caused by the slight leg movement while taking the scan, causing a loss in detail quality, which needed pre-processing filtering to improve definition. Nevertheless, a suitable fixture is readied to alleviate strain on the skin borders with minimal distortion, and additional supports are positioned beneath the thigh to minimize the creation of artifacts with the knee flexion position during the scanning process, However, it is important to mention that there were difficulties encountered when using the flexible coil device in conjunction with the MRI machine that was used for scanningscanning. The GE Medical Systems 1.5 Tesla Signa Excite MRI machine, with its 60 cm bore size, requires patients to lie, making it challenging to fit both legs into the device comfortably. This situation necessitates a slightly larger bore size for optimal functionality. Also, many coils and protocols covered all the residual limb lengths. It should also be noted that all these coils and series descriptions were tested to cover the residual limb length before performing the test on the patient.

2.1.3. 3D scanning technologies

For 3D sscanning, a white light surface scanner (Peel 3; Creaform Inc., located in Lévis, Quebec, Canada) was used to scan the patient's remaining limb. This scanner is renowned for its measurement capabilities, accurately capturing surfaces within 0.250 mm/m up to 0.1 mm and operating with a mesh resolution of 0.250 mm, scanning at a speed of 80 seconds per meter, having dimensions of 304 x 150 x 79 mm, and weighing in at 950 grams, which leads to effectively creating accurate 3D digital models.

Subsequently, the patient was scanned using a smartphone, specifically an iPhone 11 pro containing an Infrared Structured Light Projector, a TrueDepth front camera, and a 3D scanning application (Comb O&P, Chardon, OH, USA) with a scale in millimetres (mm), an Operational Scanning Range (6 - 21) in (0.16 - 0.55 M), precision up to 0.70 mm (0.03 in), and accuracy up to 1.50 mm (0.06 in).

The scanning took place in a lighted room with a temperature of 24°C, creating ideal conditions for the process. Following all the steps for 3D scanning, it took 15 minutes to scan the participant's stump. This involved preparing the scanner and conducting an inspection. Each scan lasts for around 30 seconds. A support device was used during scanning to keep the leg at an angle of about 5°.

All the 3D models obtained were post-processed in Meshmixer (Autodesk, San Rafael, California, USA) CAD software. The patient's prosthetic socket liner facilitated the smooth 3D digital reconstruction of the stump, preventing any muscular contractions or skin issues, such as suture marks resulting from the surgical operation. Hence, the reconstruction was accurate.

2.2. Accuracy and Precision of the Scanners

Six scans were taken to quantify the accuracy and the intra-rater variability (precision) with every device scanner (Peel 3, and Comb application). The accuracy of the camera systems was evaluated based on their ability to capture the shape of the residual limb compared to a reference best-fit shape (REF) as described in Table 1 of Study 1. This evaluation required aligning and combining six scans from each scanner with the CT model serving as the reference shape due to its low scanning time, high accuracy, and precision.

Six scans per system were performed on the participant to assess the precision and repeatability of the Peel 3 and COMB scans. These scans were then aligned and assembled based on the best surface fit (BEST) model alignment as detailed in Table 1 of Study 2. The analysis involved comparing scan 1 to scan 2 - 6 for the Peel 3 scanner and A to scan B-F for the COMB scan.

Distance vectors describing differences of a specific shape can be divided into four groups of points deviation, where the range from 0 mm to 1 mm is considered highly reliable, from 1 to 1.5 mm is considered reliable, from 1.5mm to 2 mm is moderately reliable, and greater than 2 mm is unreliable. So, only data points between (± 2) were computed to deal with a range in the distance vectors. The comparison has been performed in Creaform VXelementsTM (VXelements, Creaform Inc., Lévis, Quebec, Canada), which is a simple, powerful, and fully integrated 3D software platform that works in complete synergy with all 3D measurement technologies [20].

Table 1. The studies involved in the research:

Study	Measuring	Data
1	Accuracy of scanners (excluding MRI)	13 scans, three scanners, 1 Medical scan, and six scans for each 3D scanner
2	Precision of Peel 3 and COMB	12 scans, six scans per scanner

3. Results

Peel three, and the COMB scan application took six scans of the transtibial residual limb. One CT scan and one MRI scan were also taken, totaling 14 3D models (Fig. 3). The MRI scan was excluded due to the incomplete model geometry.

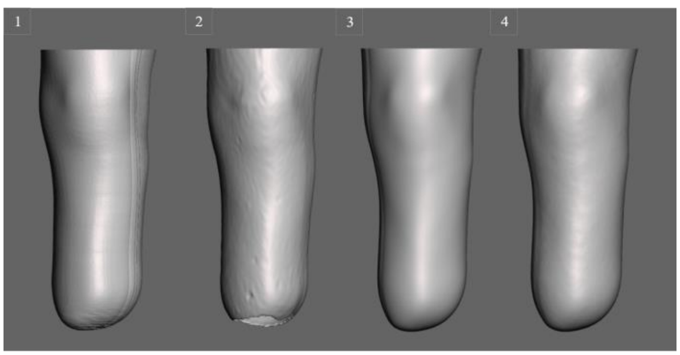

Figure 3. The three-dimensional models resulted for each system (1 CT model, 2 MRI models, 3 Peel 3 models, 4 COMB models).

3.1. Accuracy of the Scanners

A comparison of the repeat scans from the Peel 3 3D scanner against the CT scan revealed a standard deviation (SD) between ± 0.828- 0.907 Fig. 4 with the six 3D models of COMB app scans was compared subsequently to the CT scan Fig. 5. The Peel 3 3D scanner exhibited the highest surface height variance between scans and the CT scan, particularly noticeable in the frontal area of the stump. The most significant deviations were identified in the proximal-posterior region of the stump's popliteal area Fig. 6. This deviation was due to the slight change in the flexion angle between the two positions. The other notable deviation in the lateral aspect of the stump was the head of the fibula and the condyles of the tibia. On the other hand, for the COMB app, there was an apparent deviation between scans and the reference (mean standard deviation (SD) range from ± 0.823 to 0.877). The deviation is represented in the front, lateral, and posterior aspects of the stump Fig. 7. The standard deviation range for each alignment is summarised in Table 2, and the accuracy of the Peel 3 and COMB scans concerning the CT system is summarised in Table 3.

Table 2. Comparison of accuracy and precision (± mm) for Peel 3 and Comb Scanners.

3D scanner	(SD) against CT scan (accuracy)	(SD) According to Best surface fit (precision)
Peel 3	± 0.828- 0.907	± 0.531- 0.599
COMB	± 0.823- 0.877	± 0.458- 0.690

Color map 1
Alignment: Surface best fit 1

Dimensions	Tolerance	Nominal	Measured	Deviations	Tendency	Out of tol.
Min.	-1.000	0.000	-1.998	-1.998		-0.998
Max.	1.000	0.000	2.000	2.000		1.000
±	+1.000		3.998	3.998		2.998
SD	+1.000		0.907	0.907		

Color map 2
Alignment: Surface best fit 1

Dimensions	Tolerance	Nominal	Measured	Deviations	Tendency	Out of tol.
Min.	-1.000	0.000	-2.000	-2.000		-1.000
Max.	1.000	0.000	1.999	1.999		0.999
±	+1.000		3.999	3.999		2.999
SD	+1.000		0.866	0.866		

Color map 3
Alignment: Surface best fit 1

Dimensions	Tolerance	Nominal	Measured	Deviations	Tendency	Out of tol.
Min.	-1.000	0.000	-2.000	-2.000		-1.000
Max.	1.000	0.000	2.000	2.000		1.000
±	+1.000		4.000	4.000		3.000
SD	+1.000		0.828	0.828		

Color map 4
Alignment: Surface best fit 1

Dimensions	Tolerance	Nominal	Measured	Deviations	Tendency	Out of tol.
Min.	-1.000	0.000	-1.999	-1.999		-0.999
Max.	1.000	0.000	1.999	1.999		0.999
±	+1.000		3.999	3.999		2.999
SD	+1.000		0.872	0.872		

Color map 5
Alignment: Surface best fit 1

Dimensions	Tolerance	Nominal	Measured	Deviations	Tendency	Out of tol.
Min.	-1.000	0.000	-2.000	-2.000		-1.000
Max.	1.000	0.000	2.000	2.000		1.000
±	+1.000		3.999	3.999		2.999
SD	+1.000		0.866	0.866		

Color map 6
Alignment: Surface best fit 1

Dimensions	Tolerance	Nominal	Measured	Deviations	Tendency	Out of tol.
Min.	-1.000	0.000	-1.998	-1.998		-0.998
Max.	1.000	0.000	2.000	2.000		1.000
±	+1.000		3.998	3.998		2.998
SD	+1.000		0.907	0.907		

Figure 4. The standard deviation of six Peel 3 3D scanners against the reference CT scan * all the units in mm.

Color map 1
Alignment: Surface best fit 1

Dimensions	Tolerance	Nominal	Measured	Deviations	Tendency	Out of tol.
Min.	-1.000	0.000	-1.999	-1.999		-0.999
Max.	1.000	0.000	2.000	2.000		1.000
±	+1.000		3.999	3.999		2.999
SD	+1.000		0.877	0.877		

Color map 2
Alignment: Surface best fit 1

Dimensions	Tolerance	Nominal	Measured	Deviations	Tendency	Out of tol.
Min.	-1.000	0.000	-2.000	-2.000		-1.000
Max.	1.000	0.000	2.000	2.000		1.000
±	+1.000		4.000	4.000		3.000
SD	+1.000		0.823	0.823		

Color map 3
Alignment: Surface best fit 1

Dimensions	Tolerance	Nominal	Measured	Deviations	Tendency	Out of tol.
Min.	-1.000	0.000	-2.000	-2.000		-1.000
Max.	1.000	0.000	2.000	2.000		1.000
±	+1.000		4.000	4.000		3.000
SD	+1.000		0.833	0.833		

Color map 4
Alignment: Surface best fit 1

Dimensions	Tolerance	Nominal	Measured	Deviations	Tendency	Out of tol.
Min.	-1.000	0.000	-1.999	-1.999		-0.999
Max.	1.000	0.000	2.000	2.000		1.000
±	+1.000		3.999	3.999		2.999
SD	+1.000		0.850	0.850		

Color map 5
Alignment: Surface best fit 1

Dimensions	Tolerance	Nominal	Measured	Deviations	Tendency	Out of tol.
Min.	-1.000	0.000	-2.000	-2.000		-1.000
Max.	1.000	0.000	2.000	2.000		1.000
±	+1.000		4.000	4.000		3.000
SD	+1.000		0.834	0.834		

Color map 6
Alignment: Surface best fit 1

Dimensions	Tolerance	Nominal	Measured	Deviations	Tendency	Out of tol.
Min.	-1.000	0.000	-1.999	-1.999		-0.999
Max.	1.000	0.000	2.000	2.000		1.000
±	+1.000		3.999	3.999		2.999
SD	+1.000		0.840	0.840		

Figure 5. The standard deviation of six COMB scans against the reference CT scan * all the units in mm.

3.2. Precision of the Scanners

The Peel 3 3D scanner showed a low range of (SD) when five scans were aligned and compared using the best surface fit to one scan from the group where the standard deviation ranged from ± 0.531 to 0.599 (Fig. 8, left). The deviation is concentrated on the proximal-medial aspect of the stump. Some scans showed a slight deviation in the proximal lateral aspect (Fig. 9, left). On the contrary, the deviation from comparing five scans with one scan from the COMB group showed a higher percentage than the deviation of the Peel 3, which ranged from ± 0.458 to 0.690 (Fig. 8, right). The anterior proximal aspect of the stump was up to the knee joint, and the distal end of the deviation region (Fig. 9, right). Tables 4 and 5 summarise the results of precision for the two scanners.

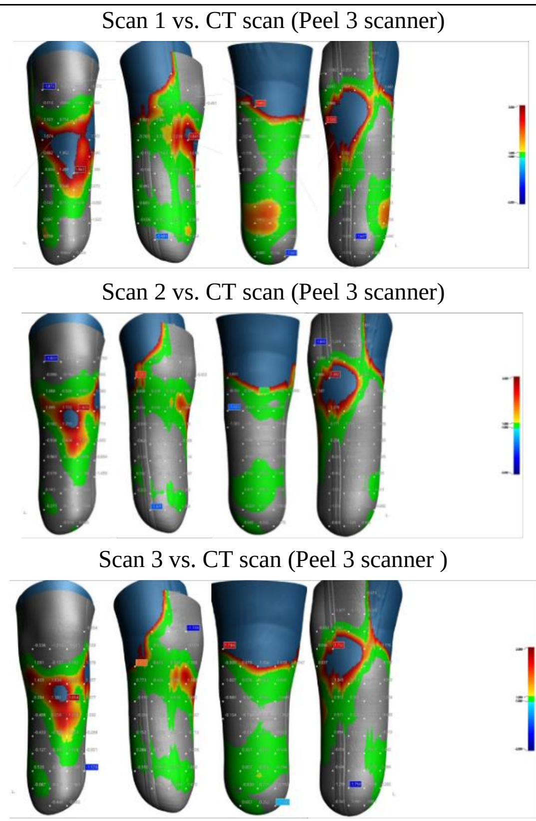

Figure 6. Peel 3 3D scanners against the reference CT scan.

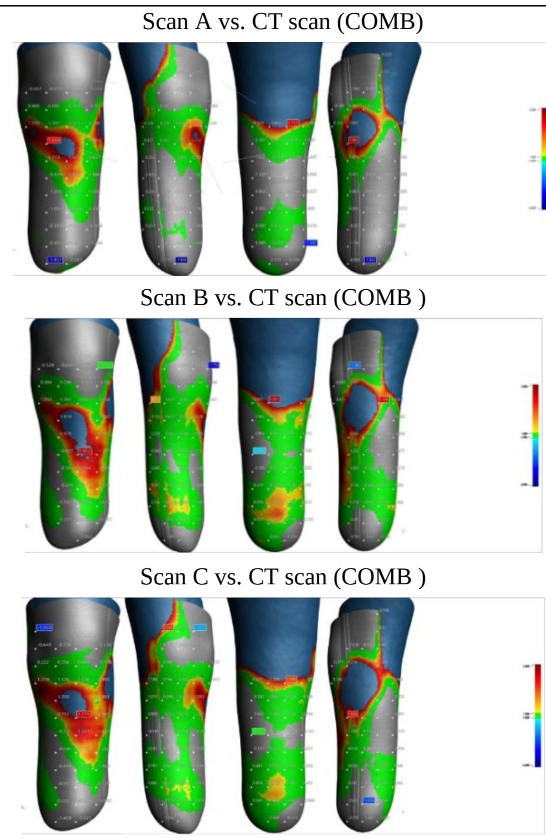

Figure 7. COMB scans against the reference CT scan.

Color map 1
Alignment: Surface best fit 1

Dimensions	Tolerance	Nominal	Measured	Deviations	Tendency	Out of tol.
Min.	-1.000	0.000	-1.998	-1.998		-0.998
Max.	1.000	0.000	2.000	2.000		1.000
±	+1.000		3.997	3.997		2.997
SD	+1.000		0.599	0.599		

Color map 2
Alignment: Surface best fit 1

Dimensions	Tolerance	Nominal	Measured	Deviations	Tendency	Out of tol.
Min.	-1.000	0.000	-2.000	-2.000		-1.000
Max.	1.000	0.000	1.994	1.994		0.994
±	+1.000		3.994	3.994		2.994
SD	+1.000		0.578	0.578		

Color map 3
Alignment: Surface best fit 1

Dimensions	Tolerance	Nominal	Measured	Deviations	Tendency	Out of tol.
Min.	-1.000	0.000	-1.998	-1.998		-0.998
Max.	1.000	0.000	2.000	2.000		1.000
±	+1.000		3.998	3.998		2.998
SD	+1.000		0.531	0.531		

Color map 4
Alignment: Surface best fit 1

Dimensions	Tolerance	Nominal	Measured	Deviations	Tendency	Out of tol.
Min.	-1.000	0.000	-1.999	-1.999		-0.999
Max.	1.000	0.000	1.999	1.999		0.999
±	+1.000		3.999	3.999		2.999
SD	+1.000		0.581	0.581		

Color map 5
Alignment: Surface best fit 1

Dimensions	Tolerance	Nominal	Measured	Deviations	Tendency	Out of tol.
Min.	-1.000	0.000	-1.998	-1.998		-0.998
Max.	1.000	0.000	2.000	2.000		1.000
±	+1.000		3.997	3.997		2.997
SD	+1.000		0.599	0.599		

Color map 1
Alignment: Surface best fit 1

Dimensions	Tolerance	Nominal	Measured	Deviations	Tendency	Out of tol.
Min.	-1.000	0.000	-1.999	-1.999		-0.999
Max.	1.000	0.000	2.000	2.000		1.000
±	+1.000		3.999	3.999		2.999
SD	+1.000		0.690	0.690		

Color map 2
Alignment: Surface best fit 1

Dimensions	Tolerance	Nominal	Measured	Deviations	Tendency	Out of tol.
Min.	-1.000	0.000	-2.000	-2.000		-1.000
Max.	1.000	0.000	1.999	1.999		0.999
±	+1.000		3.999	3.999		2.999
SD	+1.000		0.489	0.489		

Color map 3
Alignment: Surface best fit 1

Dimensions	Tolerance	Nominal	Measured	Deviations	Tendency	Out of tol.
Min.	-1.000	0.000	-1.999	-1.999		-0.999
Max.	1.000	0.000	1.999	1.999		0.999
±	+1.000		3.998	3.998		2.998
SD	+1.000		0.484	0.484		

Color map 4
Alignment: Surface best fit 1

Dimensions	Tolerance	Nominal	Measured	Deviations	Tendency	Out of tol.
Min.	-1.000	0.000	-2.000	-2.000		-1.000
Max.	1.000	0.000	1.999	1.999		0.999
±	+1.000		3.999	3.999		2.999
SD	+1.000		0.503	0.503		

Color map 5
Alignment: Surface best fit 1

Dimensions	Tolerance	Nominal	Measured	Deviations	Tendency	Out of tol.
Min.	-1.000	0.000	-2.000	-2.000		-1.000
Max.	1.000	0.000	1.709	1.709		0.709
±	+1.000		3.709	3.709		2.709
SD	+1.000		0.458	0.458		

Figure 8. (To the left) The standard deviation of Peel 3 3D scanners against one scan from the same group. (To the right) The standard deviation of COMB scans against one scan from the same group * all the units in mm.

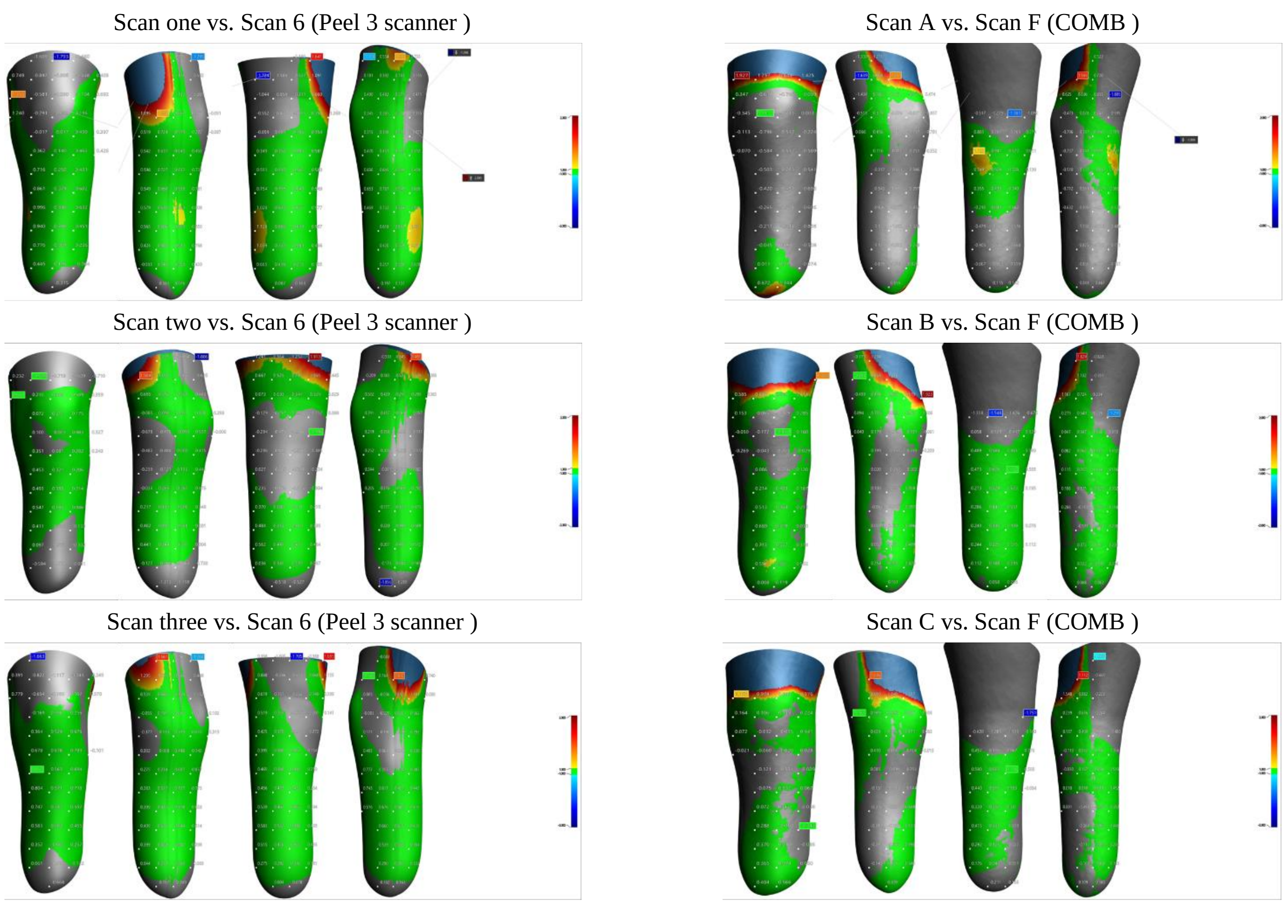

Figure 9. Peel 3 3D scanners against one scan from the same group (left), and COMB scans against one scan from the same group (right).

Table 3. The accuracy of the Peel 3 and COMB scans concerning the CT system.

Scan N.	RMS (mm), relative to the CT scan	
	Peel 3	**COMB**
1	0.907	0.877
2	0.866	0.823
3	0.828	0.833
4	0.872	0.85
5	0.866	0.834
6	0.907	0.84
Mean ± SD	0.87 ± 0.03	0.84±0.02

Table 4. The precision of the Peel scan for five scans concerning scan one from the group.

Scan pairs	Deviation (mm) Peel 3
2 vs 1	0.599
3 vs 1	0.578
4 vs 1	0.531
5 vs 1	0.581
6 vs 1	0.599
Mean ± SD	0.578 ± 0.03

Table 5. The precision of the COMB scan for five scans concerns scan A from the group.

Scan pairs	Deviation (mm) COMB
B vs A	0.69
C vs A	0.489
D vs A	0.484
E vs A	0.503
F vs A	0.458
Mean ± SD	0.525 ± 0.1

4. Discussion

The reliability of 3D scanning devices, including the Peel 3 scanner and smartphone apps like COMB, was benchmarked against CT scans to evaluate their accuracy and repeatability. The findings indicate that both the Peel 3 scanner and the smartphone-based Comb app provide sufficient accuracy and precision for clinical prosthetic applications, with performance closely aligning with CT scans. Statistical analysis revealed no significant differences between the two systems in terms of accuracy ($\chi^2 = 0.2$, $p > 0.05$). Peel 3 exhibited higher accuracy for frontal areas but showed deviations in the popliteal region. Compared with CT Peel 3, it showed high precision and reliable surface data but was sensitive to limb positioning. Despite achieving the most favourable outcomes regarding surface accuracy, the Peel 3 scanner's precision, as specified by the manufacturer, stands at 0.250 mm, aligning with its resolution of 0.250 mm. While the COMB app performed similarly, it displayed marginally higher deviations in the anterior proximal region. Compared with CT, using the Comb app on the smartphone was affordable, user-friendly, and portable, with slightly lower precision. In contrast, the MRI models suffered from incomplete geometry due to noise artifacts, limited coil compatibility, and patient discomfort during scanning, which is why the MRI model was excluded from the study. In future work, the accuracy and precision of the COMB should be investigated more to ensure the usage of this application in the prosthetic field. Acknowledging the limitations of current studies, such as small sample sizes, is crucial for understanding the generalizability of results, particularly in transtibial amputation.

5. Conclusion

This study used four different systems to create a 3D model of patients with transtibial amputation using CT, MRI, Peel 3 scanner, and smartphone. The results demonstrate that both the Peel 3 scanner and smartphone with a high-accuracy capturing camera and the presence of applications that serve the field of prosthetics, like the COMB app, are capable of accurately capturing residual limb morphology, offering viable alternatives to CT, MRI scanning and casting process in prosthetic design due to its advantageous features in terms of surface accuracy, accessibility, compact design, and user-friendly operation. The MRI was excluded due to incomplete geometry and practical challenges during scanning. At the same time, the Peel 3 scanner showed slightly higher precision for frontal and lateral areas, and the Comb app proved to be a practical and affordable option with competitive accuracy. Statistical analysis confirmed that the differences between the two systems were insignificant, making them suitable for various clinical applications. Future research should include larger sample sizes to validate these findings and explore further advancements in 3D scanning technology for prosthetic applications.

Acknowledgment

This study progressed with the support of “Baghdad Scan Medical Centre" (Baghdad, Iraq), "MULTIPATH INSPECTION “(Iraq-Erbil), and the Prosthetics and Orthotics Engineering Department laboratory (Al-Nahrain University, Jadriyah, Baghdad, Iraq).

Conflict of interest

The authors declare that there are no conflicts of interest regarding the publication of this manuscript.

Authors' contributions

Sarah Duraid AlQaissi conducted experimental and numerical analyses, drafted the original manuscript, and secured funding for the project.

Ahmed A.A. AlDuroobi: Verified the analytical methods.

Abdulkader Ali. A. Kadaw: Discussed the results and contributed to the final manuscript.

References

[1] G. M. Hobusch, K. Döring, R. Brånemark, and R. Windhager, “Advanced techniques in amputation surgery and prosthetic technology in the lower extremity,” EFORT Open Rev, vol. 5, no. 10, pp. 724–741, Oct. 2020, doi: https://doi.org/10.1302/2058-5241.5.190070.

[2] L. G. De Vivo Nicoloso, J. Pelz, H. Barrack, and F. Kuester, “Towards 3D printing of a monocoque transtibial prosthesis using a bio-inspired design workflow,” Rapid Prototyp J, vol. 27, no. 11, pp. 67–80, Dec. 2021, doi: https://doi.org/10.1108/RPJ-06-2021-0136.

[3] M. van der Stelt et al., “Pioneering low-cost 3D-printed transtibial prosthetics to serve a rural population in Sierra Leone – an observational cohort study,” EClinicalMedicine, vol. 35, p. 100874, May 2021, doi: https://doi.org/10.1016/j.eclinm.2021.100874.

[4] E. Seminati, M. Young, D. Canepa Talamas, M. Twiste, V. Dhokia, and J. Bilzon, “Reliability of three different methods for assessing amputee residuum shape and volume: 3D scanners vs. circumferential measurements,” Prosthet Orthot Int, vol. 46, no. 4, pp. 327–334, Aug. 2022, doi: https://doi.org/10.1097/PXR.0000000000000105.

[5] C. O. Squibb, M. L. Madigan, and M. K. Philen, “A high precision laser scanning system for measuring shape and volume of transtibial amputee residual limbs: Design and validation,” PLoS One, vol. 19, no. 7, p. e0301619, Jul. 2024, doi: https://doi.org/10.1371/journal.pone.0301619.

[6] W. Mehmood, N. Abd Razak, M. Lau, T. Chung, H. Gholizadeh, and N. Abu Osman, “Comparative study of the circumferential and volumetric analysis between conventional casting and three-dimensional scanning methods for transtibial socket: A preliminary study,” Proc Inst Mech Eng H, vol. 233, no. 2, pp. 181–192, Feb. 2019, doi: https://doi.org/10.1177/0954411918816124.

[7] N. Afiqah Hamzah, N. A. A. Razak, M. Sayuti Ab Karim, and H. Gholizadeh, “A review of history of CAD/CAM system application in the production of transtibial prosthetic socket in developing countries (from 1980 to 2019),” Proc Inst Mech Eng H, vol. 235, no. 12, pp. 1359–1374, Dec. 2021, doi: https://doi.org/10.1177/09544119211035200.

[8] E. Seminati, D. Canepa Talamas, M. Young, M. Twiste, V. Dhokia, and J. L. J. Bilzon, “Validity and reliability of a novel 3D scanner for assessment of the shape and volume of amputees’ residual limb models,” PLoS One, vol. 12, no. 9, p. e0184498, Sep. 2017, doi: https://doi.org/10.1371/journal.pone.0184498.

[9] L. Armitage, L. K. Kwah, and L. Kark, “Reliability and validity of the iSense optical scanner for measuring volume of transtibial residual limb models,” Prosthet Orthot Int, vol. 43, no. 2, pp. 213–220, Apr. 2019, doi: https://doi.org/10.1177/0309364618806038.

[10] Y. R. Nagarajan, F. Farukh, V. V. Silberschmidt, K. Kandan, A. K. Singh, and P. Mukul, “Shape Analysis of Prosthetic Socket Rectification Procedure for Transtibial Amputees,” Prosthesis, vol. 6, no. 1, pp. 157–174, Feb. 2024, doi: https://doi.org/10.3390/prosthesis6010013.

[11] F. Górski, R. Wichniarek, W. Kuczko, and M. Żukowska, “Study on Properties of Automatically Designed 3D-Printed Customized Prosthetic Sockets,” Materials, vol. 14, no. 18, p. 5240, Sep. 2021, doi: https://doi.org/10.3390/ma14185240.

[12] P. G. M. Knoops et al., “Comparison of three-dimensional scanner systems for craniomaxillofacial imaging,” Journal of Plastic, Reconstructive & Aesthetic Surgery, vol. 70, no. 4, pp. 441–449, Apr. 2017, doi: https://doi.org/10.1016/j.bjps.2016.12.015.

[13] P. Neri, A. Paoli, B. Aruanno, S. Barone, F. Tamburrino, and A. V. Razionale, “3D scanning of Upper Limb anatomy by a depth-camera-based system,” International Journal on Interactive Design and Manufacturing (IJIDeM), Feb. 2023, doi: https://doi.org/10.1007/s12008-023-01248-1.

[14] R. Grande, J. Albusac, D. Vallejo, C. Glez-Morcillo, and J. J. Castro-Schez, “Performance Evaluation and Optimization of 3D Models from Low-Cost 3D Scanning Technologies for Virtual Reality and Metaverse E-Commerce,” Applied Sciences, vol. 14, no. 14, p. 6037, Jul. 2024, doi: https://doi.org/10.3390/app14146037.

[15] M. Farhan, J. Z. Wang, J. Lillia, T. L. Cheng, and J. Burns, “Comparison of multiple 3D scanners to capture foot, ankle, and lower leg morphology,” Prosthet Orthot Int, vol. 47, no. 6, pp. 625–632, Dec. 2023, doi: https://doi.org/10.1097/PXR.0000000000000230.

[16] I. A. Cabrera et al., “Smartphone Telemedicine: A Novel Workflow for Creating Prosthetic Sockets Using Semi-automated Photogrammetry”, doi: https://doi.org/10.36227/techrxiv.12704984.v1.

[17] H. L. Rudy, N. Wake, J. Yee, E. S. Garfein, and O. M. Tepper, “Three-Dimensional Facial Scanning at the Fingertips of Patients and Surgeons: Accuracy and Precision Testing of iPhone X Three-Dimensional Scanner,” Plast Reconstr Surg, vol. 146, no. 6, pp. 1407–1417, Dec. 2020, doi: https://doi.org/10.1097/PRS.0000000000007387.

[18] R. Ismail et al., “Affordable and Faster Transradial Prosthetic Socket Production Using Photogrammetry and 3D Printing,” Electronics (Basel), vol. 9, no. 9, p. 1456, Sep. 2020, doi: https://doi.org/10.3390/electronics9091456.

[19] S. Cullen, R. Mackay, A. Mohagheghi, and X. Du, “The use of smartphone photogrammetry to digitise transtibial sockets: Optimisation of method and quantitative evaluation of suitability,” Sensors, vol. 21, no. 24, Dec. 2021, doi: https://doi.org/10.3390/s21248405.

[20] Y. Wakjira, N. S. Kurukkal, and H. G. Lemu, “Assessment of the accuracy of 3D printed medical models through reverse engineering,” Heliyon, vol. 10, no. 11, Jun. 2024, doi: https://doi.org/10.1016/j.heliyon.2024.e31829.